Simulating stiffness degradation and damping in soils via a simple visco-elastic-plastic model

Federico Pisanò[1] and Boris Jeremić[1,2]

[1] University of California, Davis, CA

[2] Lawrence Berkeley National Laboratory, Berkeley, CA

Abstract

Stiffness degradation and damping represent some of the most well-known aspects of cyclic soil behavior. While standard equivalent linear approaches reproduce these features by (separately) prescribing stiffness reduction and damping curves, in this paper a multiaxial visco-elastic-plastic model is developed for the simultaneous simulation of both cyclic curves over a wide cyclic shear strain range.

The proposed constitutive relationship is based on two parallel resisting/dissipative mechanisms, purely frictional (elastic-plastic) and viscous. The frictional mechanism is formulated as a bounding surface plasticity model with vanishing elastic domain, including pressure-sensitive failure locus and non-associative plastic flow – which are essential for effective stress analyses. At the same time, the use of the parallel viscous mechanism is shown to be especially beneficial to improve the simulation of the overall dissipative performance.

In order to enable model calibration on few standard experimental data, the constitutive equations are purposely kept as simple as possible with a low number of material parameters. Although the model performance is here explored with reference to pure shear cyclic tests, the multiaxial formulation is appropriate for general loading conditions.

Keywords   stiffness degradation, damping, plasticity, bounding surface, viscosity, cyclic loading

1   Introduction

Modeling soil behavior under cyclic/dynamic loading is crucial in most Geotechnical Earthquake Engineering (GEE) applications, including e.g. site response analyses and soil structure interaction (SSI) problems. In the last decades, a number of experimental studies (Ishihara, 1996; di Prisco and Wood, 2012) pointed out the complexity of such behavior – especially in the presence of pore fluid(s) – characterized by non-linearity, irreversibility, anisotropy, barotropy, picnotropy, rate-sensitivity, etc. In principle, a comprehensive soil model should be capable of reproducing all the aspects of the mechanical response for any loading condition, as well as predicting the occurrence of liquefaction and cyclic mobility, distinguishing the conditions for shakedown or ratcheting under repeated loads and so forth. However, such a perfect model is expected to require too many data for calibration, which are hardly available in most practical situations.

Conversely, many GEE problems are traditionally solved in the frequency domain by using 1D (equivalent) linear visco-elastic models, to be calibrated on standard stiffness degradation (G/G_{max}) and damping (ζ) curves. Owing to the availability of computer programs for 1D site response analysis (SHAKE (Schnabel et al., 1972), EERA (Bardet et al., 2000), DEEPSOIL (Hashash and Park, 2001)) and SSI problems (SASSI (Lysmer, 1988)), the visco-elastic approach has become more and more popular among practitioners, regardless of the following drawbacks:

- most energy dissipation in soils comes from frictional inter-granular mechanisms, rather than viscous flow;

- G/G_{max} and ζ curves do not allow to evaluate irreversible deformations, nor the influence of pore fluid(s);

- adopting 1D shear constitutive relationships has poor mechanical soundness, since soil behavior exhibits a pronounced deviatoric-volumetric coupling under general multiaxial loading conditions;

- the meaning of cyclic shear strain amplitude for the choice of G/G_{max} and ζ values is not evident in the presence of irregular seismic loads.

From the above observations the need stems for more physically consistent soil models. In the last decades, several approaches to cyclic modeling have been explored and gradually refined in the framework of elasto-plasticity, including e.g. "multi-surface plasticity", "bounding surface plasticity", "generalized plasticity" and "hypoplasticity". A number of valuable contributions are worth citing, such as – to mention only a few – Mróz et al. (1978); Prevost (1985); Wang et al. (1990); Borja and Amies (1994); Manzari and Dafalias (1997); Gajo and

Wood (1999); Papadimitriou and Bouckovalas (2002); Elgamal et al. (2003); Dafalias and Manzari (2004); Taiebat and Dafalias (2008); Andrianopoulos et al. (2010); recently, it has been also shown how a good simulation of dynamic properties can be achieved by means of even elastic-perfectly plastic models, as long as formulated in a probabilistic elastic-plastic framework (Sett et al., 2011). Comprehensive overviews on cyclic soil modeling are given by Prevost and Popescu (1996), Zienkiewicz et al. (1999) and di Prisco and Wood (2012).

As is well-known, the major issues about the practical use of elastic-plastic models concern the complexity of the mathematical formulations and the possible high number of material parameters. For a model to appeal to practicing engineers, a tradeoff is needed between the overall accuracy and the number of parameters to be calibrated, particularly provided the frequent lack of detailed *in situ* or laboratory data. This observation led the authors to set up a constitutive model with main following characteristics:

– multiaxial formulation to cope with any general stress loading condition;

– capability of reproducing the main features of soil behavior, such as stiffness reduction and damping over a wide strain range, as well as frictional failure, irreversible deformation and dilatancy;

– low number of material parameters, to be calibrated on standard experimental data and especially G/G_{max} and ζ curves.

A constitutive relationship fulfilling the above requirements is hereafter presented as the combination of two resisting/dissipative mechanism, purely frictional (elastic-plastic) and viscous. The former mechanism has been formulated starting from the work by Borja and Amies (1994), who proposed a kinematic-hardening bounding surface von Mises model for the seismic total-stress analysis of the clayey deposits at Lotung site in Taiwan (Borja et al., 1999, 2000). In particular, based on the former idea by Dafalias and Popov (1977) and Dafalias (1979), the Borja and Amies's multiaxial model is characterized by the assumption of vanishing elastic domain, implying soil plastification at any load level and a redefinition of the standard loading/unloading criterion. Recently, the vanishing elastic region approach has been also employed by Andrianopoulos et al. (2010), in order to improve the previous model by Papadimitriou and Bouckovalas (2002) with respect to numerical implementation and integration.

In this paper, a similar bounding surface approach with vanishing elastic region is exploited to derive the frictional component of the overall model in the form of a Drucker-Prager effective-stress relationship, incorporating pressure-sensitive failure and non-associative plastic flow. In addition, the model is endowed with a further viscous mechanism, which can be wisely exploited to improve the simulation of the experimental damping. Although

numerical convenience often motivates the use of viscous dissipation into elastic-plastic computations, it has a real physical origin, coming from the time-dependent processes taking place at both inter-granular contacts and grain/pore fluid interfaces.

While most model features are in fact inherited from other previous works, the proposed formulation should be considered as an attempt at reconciling traditional (linear equivalent) and advanced (elastic-plastic) cyclic modeling within an effective-stress plasticity framework. In particular, the model is shown to possess reasonable accuracy in reproducing standard modulus reduction and damping curves over a wide strain range, and it is particularly user-friendly because of the low number of material parameters. The preliminary literature survey put evidence that these advantages are not easily found in most previous effective-stress models.

In order to clearly illustrate the main modeling ingredients, the basic version of the model is hereafter presented and tested under symmetric cyclic shear loading. Its convenient mathematical structure will enable in the near future to easily remove the simplifying assumptions that, depending on the specific application, may lead to excessive inaccuracies.

2   Frictional and viscous dissipative mechanisms

The time-domain finite element (FE) solution of dynamic problems is usually carried out by solving an incremental discrete system of the following form (Bathe, 1982; Zienkiewicz and Taylor, 1991):

$$\mathbf{M}\Delta\ddot{\mathbf{U}} + \mathbf{C}\Delta\dot{\mathbf{U}} + \mathbf{K}^t\Delta\mathbf{U} = \Delta\mathbf{F}^{ext} \tag{1}$$

where Δ and dots stand respectively for step increment and time derivative, $\mathbf{U}$ is the generalized DOF vector (nodal displacement for example), $\mathbf{F}^{ext}$ the nodal external force vector and $\mathbf{M}$, $\mathbf{C}$, $\mathbf{K}^t$ are the mass, damping and (tangent) stiffness matrices, respectively.

In system (1) two dissipative sources are readily recognizable, namely the viscous (velocity-proportional) and the frictional (displacement-proportional) terms (Argyris and Mlejnek, 1991). While the latter is given by the elastic-plastic tangent stiffness $\mathbf{K}^t$, the viscous term related to the damping matrix $\mathbf{C}$ can represent interaction of solid skeleton and pore fluid, and constitutive rate-sensitiveness of the soil skeleton. The above combination of frictional and viscous dissipation can be interpreted in terms of two distinct effective stress components acting on the soil skeleton:

$$\sigma_{ij} = \sigma_{ij}^f + \sigma_{ij}^v \tag{2}$$

where the effective stress tensor σ_{ij} has been split into frictional (elastic-plastic) and viscous stresses[1]. From a rheological point of view, the resulting scheme can be defined as visco-

---

[1]Henceforth, effective stresses are exclusively accounted for

elastic-plastic. In what follows, the frictional component is first specified via the formulation of the bounding surface model with vanishing elastic domain; then, the role played by the linear viscous term is discussed.

Index tensor notation is used, along with the standard Einstein convention for repeated indices; the norm of any second-order tensor x_{ij} is defined as $\|x_{ij}\| = \sqrt{x_{ij} x_{ij}}$, whereas the deviatoric component can be extracted as $x_{ij}^{dev} = x_{ij} - x_{kk} \delta_{ij}/3$ (δ_{ij} is the Kronecker delta). In accordance with usual Solid Mechanics conventions, positive tensile stresses/strains are considered, whereas – as is done in Fluid Mechanics – only the isotropic mean pressure is positive if compressive.

2.1 Bounding surface frictional model with vanishing elastic domain

The frictional component of the model being proposed is formulated by generalizing the previous constitutive relationship by Borja and Amies (1994). In what follows, the superscript f referring to the frictional component of the global effective stress (Equation (2)) is avoided for the sake of brevity.

2.1.1 Elastic relationship

Provided the usual additive combination of (incremental) elastic and plastic strain components $d\epsilon_{ij} = d\epsilon_{ij}^e + d\epsilon_{ij}^p$, the incremental linear elastic Hooke's law is expressed as follows:

$$d\sigma_{ij} = D_{ijhk}^e \left(d\epsilon_{hk} - d\epsilon_{hk}^p \right) \Longrightarrow \begin{cases} ds_{ij} = 2G_{max} \left(de_{hk} - de_{hk}^p \right) \\ \\ dp = -K \left(d\epsilon_{vol} - d\epsilon_{vol}^p \right) \end{cases} \tag{3}$$

where d stands for a differentially small increments and D_{ijhk}^e is the fourth-order elastic stiffness tensor. Equation (3) also points out the elastic deviatoric/volumetric decoupling, in which $p = -\sigma_{kk}/3$, $\epsilon_{vol} = \epsilon_{kk}$, $s_{ij} = \sigma_{ij}^{dev}$ and $e_{ij} = \epsilon_{ij}^{dev}$ stand for mean stress, volumetric strain, stress deviator and strain deviator, respectively. The shear modulus $G_{max} = E/2 \left(1 + \nu \right)$ and the bulk modulus $K = E/3 \left(1 - 2\nu \right)$ are derived from the Young modulus E and the Poisson's ratio ν. Henceforth, G_{max} will be always used for the elastic small-strain shear modulus, whereas the secant cyclic shear stiffness will be referred to as G.

Although soil elasticity is known to be non-linearly pressure-dependent, a classical linear formulation has been here maintained to simulate constant-pressure cyclic shear tests, exclusively.

2.1.2 Drucker-Prager yield and bounding loci

A conical Drucker-Prager yield locus is first introduced, similar to what used by Prevost (1985) and Manzari and Dafalias (1997):

$$f_y = \frac{3}{2}\left(s_{ij} - p\alpha_{ij}\right)\left(s_{ij} - p\alpha_{ij}\right) - k^2 p^2 = 0 \tag{4}$$

where α_{ij} is the so called deviatoric back-stress ratio ($\alpha_{kk} = 0$) governing the kinematic hardening of the yield surface; k is a parameter determining the opening angle of the cone. The variation of the back-stress ratio α_{ij} in (4) leads to a rigid rotation of the yield locus and, therefore, a rotational kinematic hardening.

In the spirit of standard bounding surface plasticity, the yield locus must always reside within an outer surface (the so-called bounding surface), here assumed in the form of a further Drucker-Prager cone (non kinematically hardening, fixed in size):

$$f_B = \frac{3}{2}s_{ij}s_{ij} - M^2 p^2 = 0 \tag{5}$$

where M provides the bounding cone opening and, as a consequence, the material shear strength.

2.1.3 Plastic flow and translation rules

The plastic flow of soils is in general non-associative (Nova and Wood, 1979) and gives rise to plastic contractancy or dilatancy depending on whether loose or dense materials are considered. Here, the plastic flow rule is borrowed from Manzari and Dafalias (1997):

$$d\epsilon^p_{ij} = d\lambda\left(n^{dev}_{ij} - \frac{1}{3}D\delta_{ij}\right) \tag{6}$$

where $d\lambda$ is the plastic multiplier, n^{dev}_{ij} is a deviatoric unit tensor ($\|n^{dev}_{ij}\| = 1$) and D is a dilatancy coefficient defined as (Manzari and Dafalias, 1997):

$$D = \xi\left(\alpha^d_{ij} - \alpha_{ij}\right)n^{dev}_{ij} = \xi\left(\sqrt{\frac{2}{3}}k_d n^{dev}_{ij} - \alpha_{ij}\right)n^{dev}_{ij} \tag{7}$$

in which ξ and k_d are two positive constitutive parameters. While the former controls the amount of volumetric plastic strain, the latter determines the position of the so called "dilatancy surface" and rules the transition from contractive ($D > 0$) to dilative ($D < 0$) behavior under undrained triaxial conditions[2].

---

[2]Under different loading conditions this transition is not "exactly" governed only by the location of the current stress state with respect to the dilatancy surface

For the sake of simplicity (and regardless of some experimental evidences), the kinematic hardening evolution of the yield locus and the direction of the deviatoric plastic strain increment are related through the standard Prager's rule (Borja and Amies, 1994):

$$d\alpha_{ij} = \|d\alpha_{ij}\| n_{ij}^{dev} \tag{8}$$

2.1.4   Vanishing elastic region

As previously mentioned, the main feature of the frictional model concerns the vanishing elastic domain, corresponding with the limit $k \to 0$ in Equation (4). Accordingly, the Drucker-Prager cone reduces to its axis, so that:

$$\lim_{k \to 0} f_y = 0 \Rightarrow \frac{s_{ij}}{p} = r_{ij} = \alpha_{ij} \Rightarrow d\alpha_{ij} = dr_{ij} = \frac{ds_{ij}}{p} - \frac{s_{ij}}{p^2} dp \tag{9}$$

where r_{ij} is the deviatoric stress ratio tensor (Manzari and Dafalias, 1997). After substituting the Prager's rule (8) into (9) it results:

$$n_{ij}^{dev} = \frac{dr_{ij}}{\|dr_{ij}\|} = \frac{ds_{ij} - \alpha_{ij} dp}{\|ds_{ij} - \alpha_{ij} dp\|} \tag{10}$$

From Equation (10) it can be inferred that:

1. since the direction of the plastic strain increment overall depends on the stress increment $d\sigma_{ij}$, the resulting constitutive formulation is by definition "hypoplastic" (Dafalias, 1986);

2. hydrostatic stress increments ($ds_{ij} = 0$) from initial hydrostatic states ($\alpha_{ij} = 0$) produce $n_{ij}^{dev} = 0 \to \epsilon_{ij}^{dev} = 0$;

3. the deviatoric plastic strain increment is along the direction of the deviatoric stress ratio increment. This directly comes from the use of the above Prager's rule in combination with the vanishing elastic region. Although this finding is not in full agreement with general experimental evidences, it will not prevent satisfactory cyclic G/G_{max} and ζ curves to be obtained.

Starting from Equation (9), the norm $\|d\alpha_{ij}\| = \|dr_{ij}\|$ can be specified for the case of radial loading paths in the deviatoric plane, which are characterized by $dp = 0$ and the coaxiality of s_{ij} and ds_{ij}. Under these loading conditions, simple manipulations lead to find:

$$\|d\alpha_{ij}\| = \sqrt{\frac{2}{3}} \frac{dq}{p} \tag{11}$$

where $q = \sqrt{3/2}\|s_{ij}\|$ stands for the usual deviatoric stress invariant.

2.1.5 Hardening relationship and plastic multiplier

An incremental hardening relationship is directly established (Borja and Amies, 1994):

$$dq = \sqrt{\frac{2}{3}} H \| de_{ij}^p \| \tag{12}$$

where H is the hardening modulus. Then, the substitution of both the flow rule (6) and the hardening relationship (12) into (11) leads to:

$$\| d\alpha_{ij} \| = \frac{2}{3} \frac{H d\lambda}{p} \tag{13}$$

By equaling the two definitions of ds_{ij} arising from Equations (3)-deviatoric and (9), and then using Equations (3)-volumetric and (13) the following relationship is obtained:

$$2G_{max} \left(de_{ij} - d\lambda n_{ij}^{dev} \right) = \| d\alpha_{ij} \| n_{ij}^{dev} p + \alpha_{ij} dp = \frac{2}{3} \frac{H d\lambda}{p} n_{ij}^{dev} p - \alpha_{ij} K \left(d\epsilon_{vol} + d\lambda D \right) \tag{14}$$

whence:

$$d\lambda = \frac{2G_{max} de_{ij} n_{ij}^{dev} + K d\epsilon_{vol} \alpha_{ij} n_{ij}^{dev}}{2G + \frac{2}{3}H - K D \alpha_{ij} n_{ij}^{dev}} \tag{15}$$

Equation (15) represents the consistent frictional generalization of Equation (18) in Borja and Amies (1994), as well as the limit of Equation (12) in Manzari and Dafalias (1997)[3] for a vanishing size of the yield locus.

2.1.6 Projection rule, hardening modulus and unloading criterion

The theory of bounding surface plasticity relies on the basic concept that the plastic modulus explicitly depends on the distance between the current stress state and an *ad hoc* stress projection onto the bounding surface. On this issue, benefits and pitfalls of different projection rules have been thoroughly discussed by Andrianopoulos et al. (2005).

Here, the stress projection in the π-plane (deviatoric stress ratio plane) is assumed to be along the direction of $\alpha_{ij} - \alpha_{ij}^0$:

$$\alpha_{ij}^b = \alpha_{ij} + \beta \left(\alpha_{ij} - \alpha_{ij}^0 \right) \tag{16}$$

where β is a scalar distance coefficient, while α_{ij}^0 is the back-stress ratio at the last loading reversal (Figure 1). As observed by Andrianopoulos et al. (2010), projection rules of the

---

[3]Different signs result because of the opposite sign conventions adopted by these authors

type (16) are "stable", in the sense that small perturbations of the loading direction do not affect severely the location of the stress projection on the bounding surface.

The coefficient β is obtained by enforcing the projected stress σ_{ij}^b to lie on the bounding surface (Equation (5)):
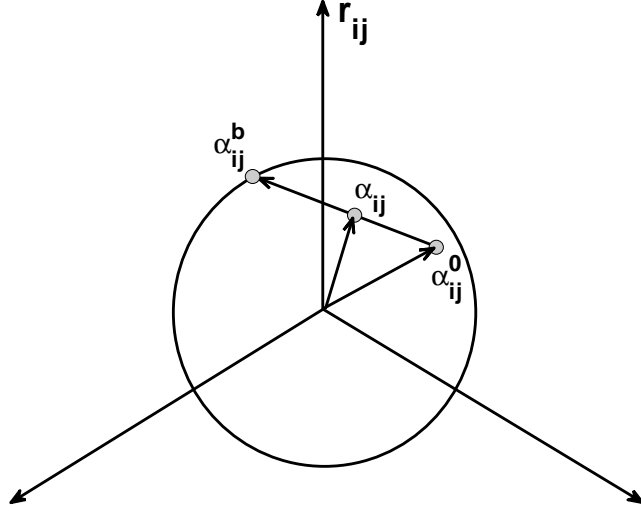
Figure 1: Representation of the projection rule (16)

$$\frac{3}{2} s_{ij}^b s_{ij}^b = M^2 \left(p^b\right)^2 \iff \frac{3}{2} \alpha_{ij}^b \alpha_{ij}^b = M^2 \tag{17}$$

that is by substituting (16) into (17) and then deriving the positive root of the following algebraic equation[4]:

$$\left\|\alpha_{ij} - \alpha_{ij}^0\right\|^2 \beta^2 + 2\alpha_{ij}\left(\alpha_{ij} - \alpha_{ij}^0\right)\beta + \left\|\alpha_{ij}\right\|^2 - \frac{2}{3}M^2 = 0 \tag{18}$$

The analytical relationship between H and β is chosen to fulfill the following requirements:

1. $H\left(\beta = 0\right) = 0$, that is full mobilization of the material strength when the stress image point lies on the bounding surface;

2. $H\left(\beta \to \infty\right) \to \infty$, that is (instantaneous) recover of the elastic stiffness at the onset of load reversal (i.e. $\alpha_{ij} = \alpha_{ij}^0$).

---

[4]The adoption of a simple Drucker-Prager-type bounding surface allows β to be analytically obtained. This would not be the case in the presence of more complex π-sections

In this case, the following $H - \beta$ relationship has been introduced because of its simplicity:

$$H = ph\beta^m \tag{19}$$

in which h and m are two additional constitutive parameters.

In the absence of a finite-sized elastic region, the occurrence of unloading cannot be checked by comparing the loading direction and the local normal to the yield locus. This requires the difinition of an alternative unloading criterion, coinciding here with providing a rule for updating α_{ij}^0. Borja and Amies (1994) proposed a criterion based on the observation that the hardening modulus H increases at the onset of unloading, so that – as long as $H(\beta)$ is a monotonically increasing function – instantaneous unloading is assumed whenever $dH > 0$, i.e. $d\beta > 0$. However, the authors experienced that such an unloading criterion lacks robustness in numerical computations under complex/irregular loading paths, because the small values assumed by β (especially close to the bounding surface) can be easily corrupted even by numerical inaccuracies; as a result, unrealistic unloading is often likely to arise. While different proposals are available in literature to overcome this problem (Andrianopoulos et al., 2005, 2010), the following unloading criterion has been here preferred:

$$\left(\alpha_{ij} - \alpha_{ij}^0\right) dr_{ij} < 0 \iff \left(\alpha_{ij} - \alpha_{ij}^0\right) n_{ij}^{dev} < 0 \tag{20}$$

in which the coaxiality of $d\alpha_{ij} = dr_{ij}$ and n_{ij}^{dev} (Prager's rule (8)) has been exploited.

It should be also borne in mind that this kind of updating criterion is likely to give rise to "overshooting" phenomena under general loading paths (Dafalias, 1986). Overshooting takes place when, after loading along a given direction, a very small unloading implies an updated α_{ij}^0 before reloading along the original direction. The updated small distance between the current and the reversal stresses determines an unrealistically high reloading stiffness, so that "the corresponding stress-strain curve will overshoot the continuation of the previous curve which would have occurred if no unloading/reverse loading/reloading had taken place" (Dafalias, 1986). While this shortcoming can be usually observed under irregular seismic loading, it will not be detected in the results being presented, exclusively concerning symmetric sinusoidal cyclic loading. A recent discussion on the remediation of overshooting is provided by E-Kan and Taiebat (2014).

2.1.7 Possible refinements

The frictional model has been developed trying to keep the number of material parameters as low as possible, even with a non-associated flow rule. However, it is worth mentioning which kind of improvements might be introduced if required by the problem under examination.

It should be first noted that, as a Drucker-Prager type bounding surface has been adopted, the material shear strength is unaffected by the Lode angle, so that for instance the

same failure obliquity is predicted for triaxial compression and extension. This drawback could be easily remedied by modifying the deviatoric cross-section of the bounding surface itself, e.g. by adopting the well known Mohr-Coulomb deviatoric locus or other smooth loci (Matsuoka and Nakai, 1974; Willam and Warnke, 1974; Lade, 1977). A change in the deviatoric cross-section would negligibly influence the overall formulation, as just the evaluation of the projection distance β (Equation (17)).

Secondly, the present version of the model cannot predict a possible softening behavior of the soil, usually taking place in the case of dense materials. Softening could be accounted for by incorporating a further isotropic hardening mechanism at the bounding surface level, allowing for a gradual shrinkage of the outer surface during plastifications.

Another relevant point concerns the fact that different parameters must be calibrated for different void ratios of the same granular material, as if distinct materials were indeed considered. As a matter of fact, continuous transitions from loose to dense states (and vice versa) spontaneously take place during straining: this aspect has been successfully addressed and reproduced via the concept of "state parameter" (Been and Jefferies, 1985; Wood et al., 1994; Manzari and Dafalias, 1997), which could be also introduced into a critical-state version of the proposed model. Also, the state parameter concept represents a natural way to reproduce softening as an effect of the material evolution from peak strength to critical state conditions.

While the above aspects concern both monotonic and cyclic loading conditions, further issues could be addressed with more specific reference to cyclic/dynamic loading, as for instance fabric effects (Papadimitriou and Bouckovalas, 2002; Dafalias and Manzari, 2004) and anisotropy, the evolution toward shakedown or ratcheting under a large number of loading cycles (di Prisco and Wood, 2012), the occurrence of cyclic mobility (Elgamal et al., 2003), rate-sensitiveness and related frequency effects.

Apparently, refining the model formulation in the light of the above observations would result in more accurate predictions/simulations, implying though higher difficulties in terms of calibration, implementation and, as a consequence, practical employment. Conceiving a model reasonably accurate but still "user-friendly" is the main goal of the present study, in order to provide engineers with a tool fitting standard cyclic modeling concepts (modulus reduction and damping curves) in a 3D elastic-plastic fashion. Accordingly, while looking for a compromise between accuracy and simplicity, some experimental evidences have been purposely disregarded on the modeling side.

2.2   The role of linear viscous damping

An additional viscous mechanism (Equation (2)) is usually available exploited in most finite element (FE) codes, even though it is not directly included in the constitutive model. Indeed,

many numerical programs solve discrete systems with a viscous damping term (Equation (1)), usually assembled as a linear combination of the mass and the (elastic) stiffness matrices (Rayleigh formulation (Argyris and Mlejnek, 1991; Chopra, 2000)):

$$\mathbf{C} = a_0\mathbf{M} + a_1\mathbf{K}^e \tag{21}$$

where a_0 and a_1 are two constant parameters, related to the nth modal damping ratio ζ_n of the discrete structural system.

It could be easily shown that a constitutive viscosity in the form:

$$\sigma_{ij}^v = D_{ijhk}^v \dot{\epsilon}_{hk} \tag{22}$$

gives rise to a stiffness-proportional damping matrix, which can be equivalently reproduced through the following calibration of the Rayleigh damping parameters (Borja et al., 2000; Hashash and Park, 2002):

$$a_0 = 0 \qquad a_1 = \frac{2\zeta_0}{\omega} \tag{23}$$

The calibration (23) establishes the same ratio between tangential/bulk elastic and the viscous moduli, that is $G_{max}^e/G_{max}^v = K^e/K^v$. More importantly, a damping ratio ζ_0 is ensured for a given circular frequency ω, as long as the parallel resisting mechanism (σ_{ij}^f) is purely elastic; as a consequence, provided the a_1 value at the beginning of the analysis, modal frequencies and the corresponding damping ratios are linearly related.

It is also worth remarking some further points about the implications of linear viscous damping in conjunction with non-linear soil models. If a soil element undergoes an imposed shear strain history, the overall shear stress/strain cycles $\tau-\gamma$ differ from the purely frictional component $\tau^f-\gamma$, this difference being due to the viscous shear stress τ^v. As will be shown in next section, the viscous component implies smoother cycles and avoid the sharp transitions at stress reversal usually exhibited by purely elastic-plastic responses (Borja et al., 2000). However, the overall G/G_{max} ratio between the average cyclic stiffness and the elastic shear modulus is unaffected by viscosity.

As far as the damping ratio is concerned, its standard definition (Kramer, 1996) can be easily adapted to point out the frictional/viscous splitting of the energy ΔW dissipated in a loading cycle:

$$\zeta = \frac{\Delta W}{2\pi G\gamma_{max}^2} = \frac{\Delta W^f + \Delta W^v}{2\pi G\gamma_{max}^2} = \zeta^f + \zeta^v \tag{24}$$

where γ_{max} is the imposed cyclic shear strain amplitude and G the corresponding (secant) cyclic shear stiffness. As γ_{max} approaches zero, the plastic dissipation tends to zero as well, so that $\zeta = \zeta^v$; therefore, the Rayleigh parameter a_1 can be calibrated to obtain $\zeta(\gamma_{max} \to 0) = \zeta_0$ for a given circular frequency ω (see Equation (23)). This is a desirable

feature of the model, as natural soils are well known to dissipate energy at even very small strain amplitudes.

At progressively larger strains, both the frictional and viscous components contribute to the global damping, although the relative quantitative significance is hard to assess *a priori*. In addition, the viscous component of the $\zeta - \gamma_{max}$ curve is not constant, since ζ^v depends on the strain-dependent secant modulus $G(\gamma_{max})$ and, implicitly, on the strain rate. This is different to what has been argued by Borja et al. (2000).

As an example, consider the response of an elastic-perfectly plastic model with additional viscosity under a sinusoidal shear excitation $\gamma(t) = \gamma_{max} \sin(\omega t)$. The simplicity of the elastic-perfectly plastic response allows derivation of instructive analytical formulas for the G/G_{max} and the damping ratios, even in the presence of viscous dissipation. While $\gamma_{max} < \gamma_y$ (yielding shear strain), the material behavior is linear elastic, so that $G/G_{max} = 1$ and ζ equals the purely viscous contribution at $\gamma_{max} = 0$, i.e. $\zeta = \zeta_0$; γ_y depends on the elastic stiffness and the shear strength of the material, $\gamma_y = \tau_{lim}/G_{max}$, where τ_{lim} is the limit (frictional) shear stress for a given confining pressure. For $\gamma_{max} > \gamma_y$ plastifications take place with a flat elastic-perfectly plastic $\tau^f - \gamma$ branch, and the following expressions can be easily derived:

$$\frac{G}{G_{max}} = \frac{\tau_{lim}}{G_{max}\gamma_{max}} \tag{25}$$

$$\zeta = \frac{\Delta W^f + \Delta W^v}{2\pi G \gamma_{max}^2} = \underbrace{\frac{2}{\pi}\left(1 - \frac{\tau_{lim}}{G_{max}\gamma_{max}}\right)}_{\zeta^f} + \underbrace{\zeta_0 \frac{G_{max}\gamma_{max}}{\tau_{lim}}}_{\zeta^v} \tag{26}$$

In Figure 2 the G/G_{max} and ζ ratios are plotted for increasing ζ_0 values. As γ_{max} increases, the frictional damping tends to $2/\pi \approx 0.63$, while the viscous one keeps increasing because of the reduction in the secant stiffness and the increase in the shear strain rate (depending on the strain amplitude). Hence, the value of ζ_0 is to be carefully chosen, in order to avoid excessive dissipation when medium/large strains are induced by the loading process.

The fact that the viscous mechanism can modify the purely frictional $\zeta - \gamma_{max}$ curve without altering the cyclic stiffness degradation can be fruitfully exploited to improve experimental-numerical agreement in terms of energy dissipation.

3 Model performance and calibration

The frictional mechanism of the above model is characterized by a very low number of material parameters, namely the following seven:
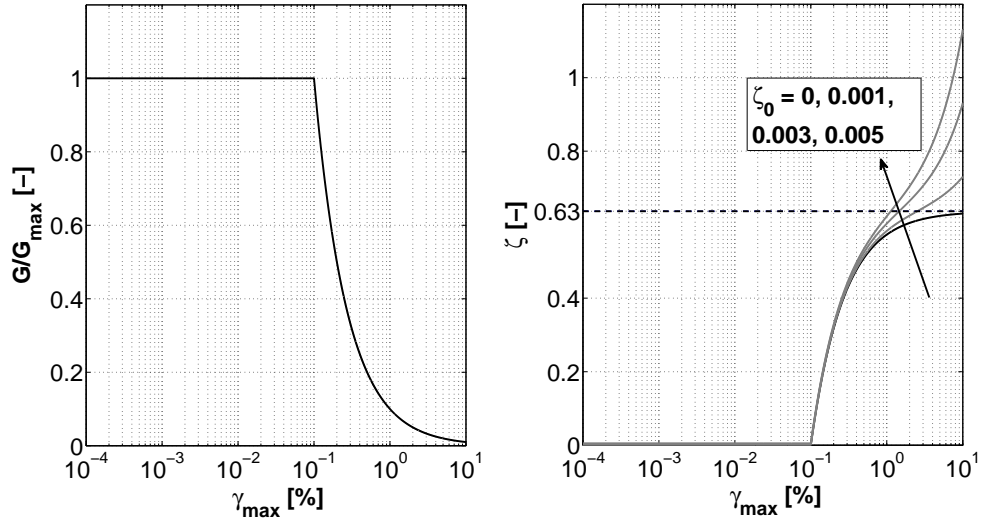
Figure 2: G/G_{max} and damping curves for a elastic-perfectly plastic model with linear viscous damping at varying ζ_0 (τ_{lim}=100 kPa, G_{max}=100 MPa)

- two elastic parameters, the Young modulus E (or the shear modulus G_{max}) and the Poisson's ratio ν;

- the shear strength parameter M for the definition of the bounding surface (Equation (5));

- the flow rule parameters, ξ and k_d, governing the increment of the volumetric plastic strain under shearing and the size of the dilatancy surface, respectively (Equation (6));

- the hardening parameters h and m for the dependence of the hardening modulus on the distance coefficient β (Equation (19)), affecting the pre-failure deformational behavior and, in overall, the resulting dynamic properties (G/G_{max} and damping curves).

Provided a reasonable value for the Poisson's ratio (usually in the range $0.25 - 0.4$), the small-strain elastic stiffness can be evaluated from dynamic laboratory (RC tests) or *in situ* (seismic geophysical surveys) tests. As far as the shear strength is concerned, the parameter M can be related to the friction angle ϕ as follows:

$$M = \frac{6\sin\phi}{3 \pm \sin\phi} \tag{27}$$

to reproduce triaxial compression (sign $-$ in (27)) or extension (sign $+$ in (27)) failure conditions. While different bounding deviatoric sections would easily capture both compressive and extensive limits (Manzari and Dafalias, 1997), the calibration of a circular deviatoric locus can be tackled – as usual – by setting a trade-off M in between the bounding values

14

in Equation (27) (this is appropriate, for instance, for plane strain problems). Also, since no strain-softening is reproduced, the peak strength or the residual ϕ is to be considered on the basis of the specific purpose of the analysis, i.e. depending on whether optimistic or safe assessments are needed. In any case, the present version of the model is not well suited for problems where simulating failure is particularly relevant (e.g. slope stability analyses).

The calibration of the flow rule parameters, ξ and k_d, requires at least a triaxial test to be performed, in order to obtain some information about the volumetric behavior. In particular, under undrained triaxial conditions, k_d coincides with the stress ratio ($\eta = q/p'$) characterizing the so-called "phase transformation line" (Ishihara et al., 1975) and determining the compactive/dilative transition. In the case of loose (compactive) materials, since fixed bounding and dilatancy surfaces are considered in this version of the model, $k_d = M$ is set to ensure a compactive behavior vanishing as the limit external locus is achieved. Figure 3 shows the predicted triaxial response for three different values of k_d (and fixed ξ), that is by varying the opening angle of the dilatancy surface (the employed parameters are reported in the figure caption, where p_0 stands for the initial mean pressure).

While the limit stress deviator q is exclusively given by M, the pre-failure behavior is influenced by the plastic deformability and therefore by k_d. The model possesses sufficient flexibility to reproduce contractive, dilative or contractive/dilative behavior; also, such a feature is necessary to reproduce undrained conditions (liquefying and non-liquefying responses), this being a further motivation for non-associativeness when dealing with sandy materials.

Figure 4 exemplifies the response predicted under pure shear (PS) cyclic loading, applied as a sinusoidal shear strain history ($\gamma_{max} = 0.2\%, 20\%$, period $T=2\pi$ s) at constant normal stresses (and thus constant mean pressure p_0 as well). This corresponds with a radial loading path on the deviatoric plane); for the sake of clarity, the volumetric plastic response has been inhibited ($\xi=0$), in order to evaluate the deviatoric mechanism exclusively. Both purely frictional (solid line) and frictional/viscous (dashed line) responses are plotted.

Owing to the kinematic hardening of the vanished yield locus, the model can reproduce both the Bauschinger and the Masing effects, the latter implying the stabilization of the cyclic response to take place after more than one loading cycle. As expected, the additional viscous damping increases the area of the cyclic loop and therefore the overall dissipated energy; however, the effect of the viscous dissipation becomes significant only at medium-high shear strains, corresponding – for a given loading frequency – with higher strain rates. Further, viscosity causes the aforementioned "smoothing" of stress reversals, as it can be noticed in Figure 5 by comparing the purely frictional and the frictional/viscous responses.

Given the elastic stiffness and the strength of the soil, the shape of the resulting loading cycles is totally governed by the hardening properties, by h and m in Equation (19): this
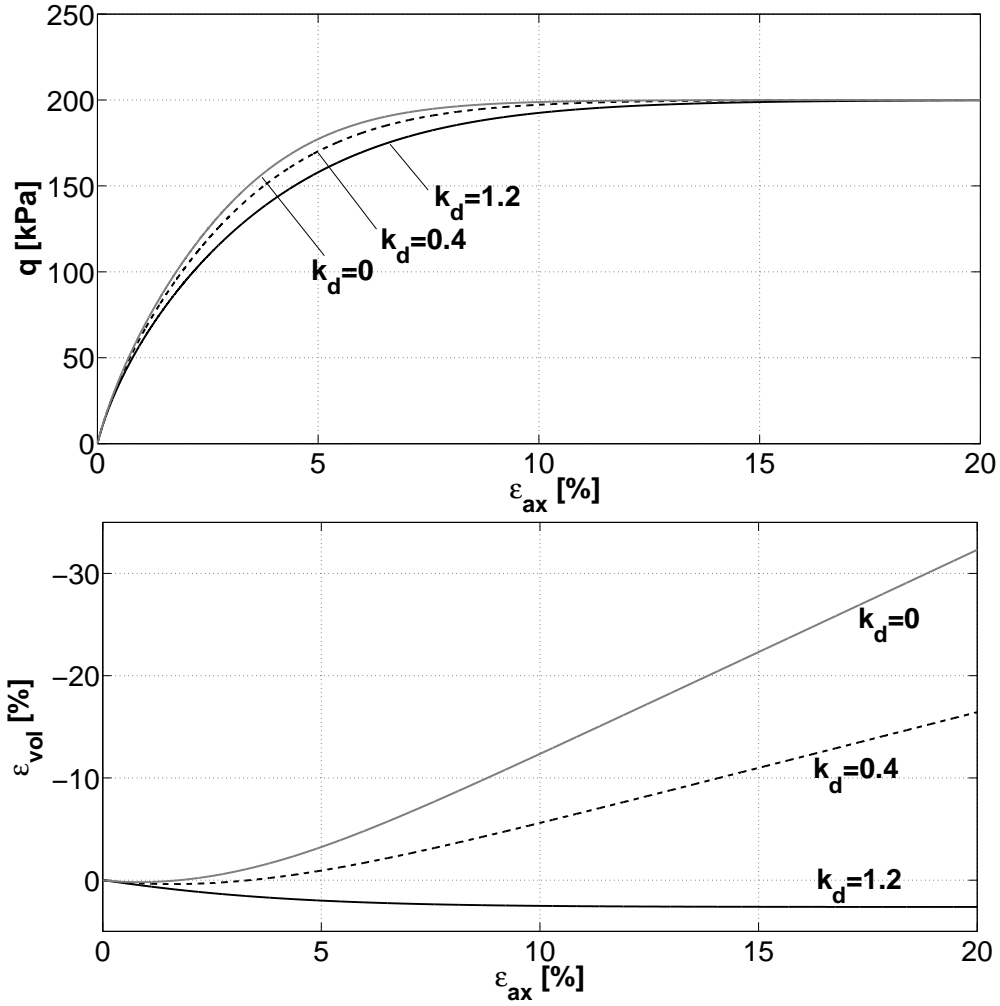
Figure 3: Predicted triaxial responses for different dilatancy surfaces (p_0=100 kPa, G_{max} = 4 MPa, ν=0.25, M=1.2, ξ=1, h=$G/(1.5p_0)$, m=1)

directly affects the simulation of experimental G/G_{max} and damping curves, which can be therefore exploited for the calibration of both h and m. As is proven in Appendix A, the following equality holds under PS loading conditions:

$$1 = \frac{G}{G_{max}} \left[1 + \frac{6G_{max}}{hp_0\gamma_{max}} \int_0^{\gamma_{max}} \left(\frac{\gamma}{\tau_{lim}/G - 2\gamma + \gamma_{max}} \right)^m d\gamma \right] \tag{28}$$

where $\tau_{lim} = Mp_0/\sqrt{3}$. Relationship (28) has been obtained by integrating the constitutive equations over the first loading cycle, and represents the frictional counterpart of Equation (6) in Borja et al. (2000) – as is testified by the explicit influence of the confining pressure p_0. The proper use of Equation (28) requires first the choice of two meaningful points on the G/G_{max} experimental curve, i.e. two (γ_{max}, G/G_{max}) couples; then, the unknowns h and m are obtained by solving the integral system arising from the specification of Equation (28)

16
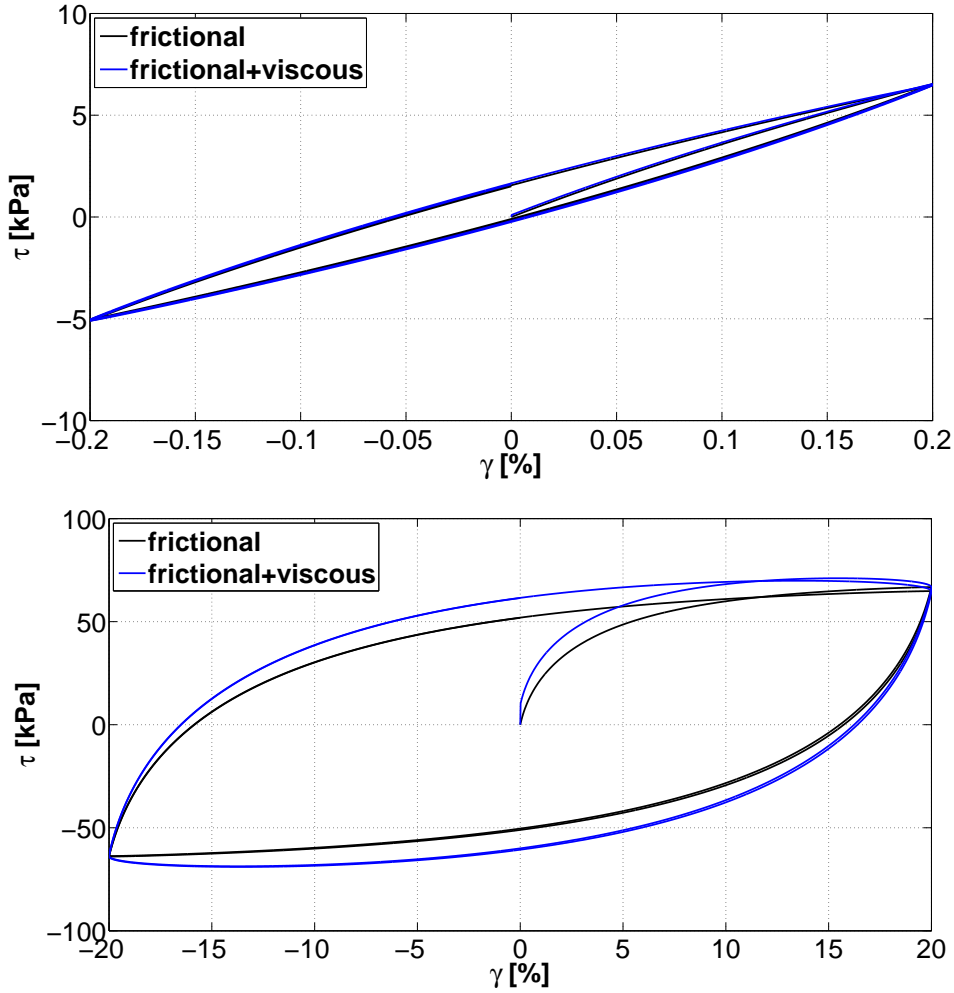
Figure 4: Predicted pure shear response at two different shear strain amplitudes (p_0=100 kPa, T=2π s, $\zeta_0 = 0.006$, G_{max}= 4 MPa, ν=0.25, M=1.2, k_d=ξ=0, h=$G/(1.5p_0)$, m=1)

for both selected $(\gamma_{max}, G/G_{max})$ couples.

Figure 6 illustrates the result of the above calibration procedure, applied on the G/G_{max} and ζ curves for sands implemented into the code EERA (Bardet et al., 2000) and formerly obtained by Seed and Idriss (1970).

Since Equation (28) exclusively accounts for the G/G_{max} curve, the very satisfactory agreement in terms of stiffness degradation (viscosity has no effect on it) should not surprise. On the other hand, once h and m are set, the predicted damping curve may or may not match the experimental outcome irrespective of the calibration procedure. In this respect, Figure 6 also presents the comparison between the damping curve by Seed and Idriss and the model prediction. The frictional ζ curve lies in the same experimental range, even though the accuracy at $\gamma_{max} = 0.03 - 1\%$ is not as good as for the G/G_{max} ratio. In this case, the
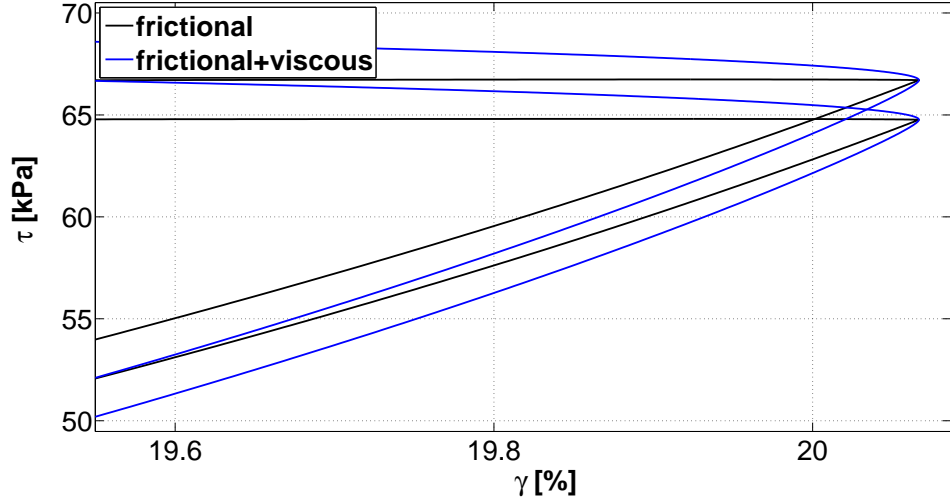
Figure 5: Detail of stress reversals for the pure shear response in Figure 4 ($\gamma_{max} = 20\%$)
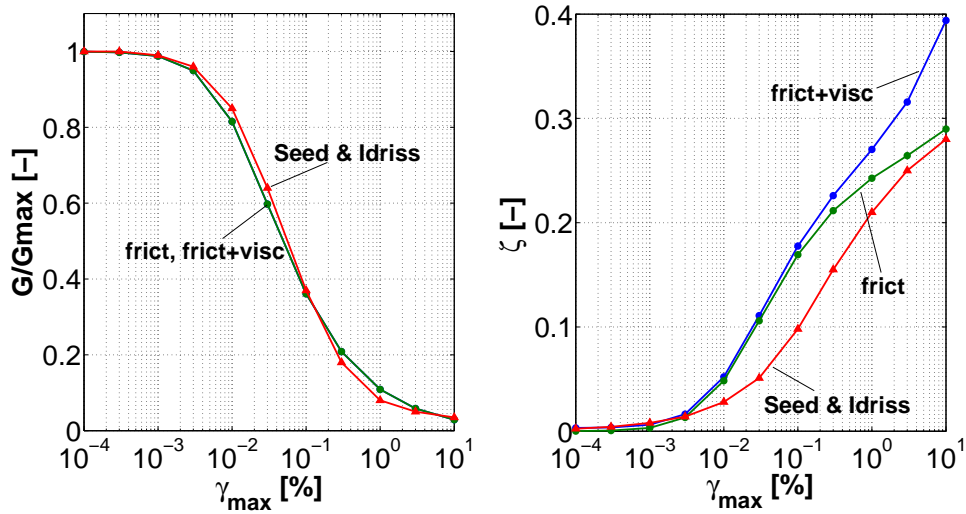
Figure 6: Comparison between experimental and simulated G/G_{max} and damping curves (p_0=100 kPa, T=2π s, $\zeta = 0.003$, $G_{max} = 4$ MPa, ν=0.25, M=1.2, k_d=ξ=0, h=$G/(112p_0)$, m=1.38)

contribution of the viscous mechanism is practically non-existent, as it only increases the total ζ ratio for $\gamma_{max} > 0.1\%$.

Depending on the specific application, a "trial and error" calibration might be preferable, sacrificing some of the accuracy in terms of G/G_{max} ratio to improve the damping performance. A possible outcome of a manual calibration is plotted in Figure 7: apparently, while the simulation of the stiffness curve is still acceptable, the damping curve appears to be much better than the previous one. The use of the viscous mechanism seems to be highly

beneficial, since it remedies the lack of accuracy in the frictional curve at medium/large cyclic strains.
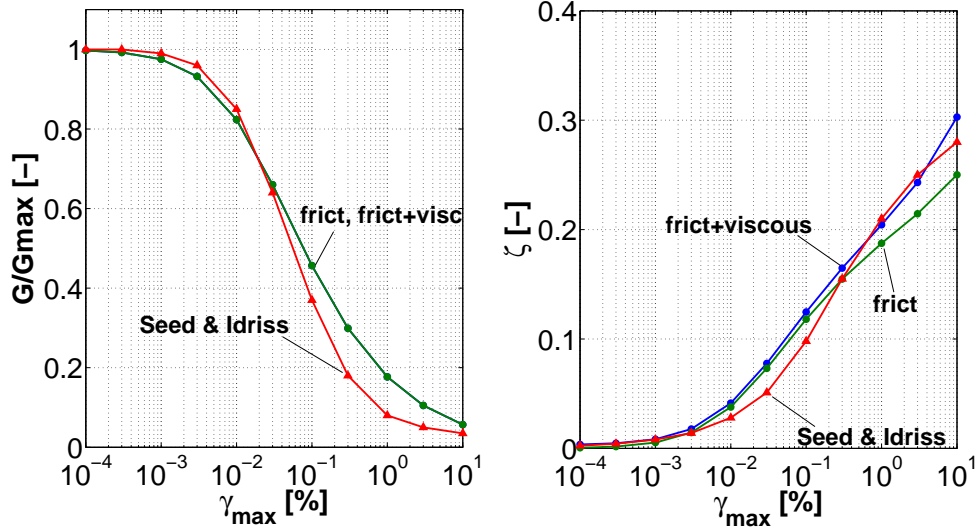
Figure 7: Comparison between experimental and simulated G/G_{max} and damping curves (p_0=100 kPa, T=2π s, $\zeta = 0.003$, $G_{max} = 4$ MPa, ν=0.25, M=1.2, k_d=ξ=0, h=$G_{max}/(15p_0)$, m=1)

It is also worth noting that the experimental/numerical agreement is satisfactory up to even $\gamma_{max} = 10\%$, where substantial plasticity occurs and, in any case, the extrapolation of cyclic curves from experimental data is – to say the least – questionable.

Besides, if the experimental data under examination are unsatisfactorily reproduced for any h and m combination, the user still has the chance of substituting the interpolation function (19) with no further changes in the model formulation. In particular, the present model is as flexible as the one by Borja and Amies (1994) in reproducing, for a given initial mean pressure, usual 1D non-linear laws for soils, such as the exponential, the hyperbolic, the Davidenkov and the Ramberg-Osgood models (for this latter a hardening bounding surface would be needed as well). Matching the aforementioned 1D laws ensures sufficient capability of reproducing experimental curves of usual shape.

4 Parametric analysis

In this section the influence of some relevant input parameters on the model predictions is parametrically investigated.

4.1 Influence of the confining pressure

Figure 8 illustrates the sensitivity, under PS loading, of both G/G_{max} and damping frictional curves to the initial confining pressure. As can be noticed, increasing p_0 does enlarge the "pseudo-elastic" range, that is the strain interval within which the deviation by the elastic behavior is negligible even with a vanishing yield locus. It is also noted that the variations in the confining pressure do not imply appreciable changes in the shape of the curves.
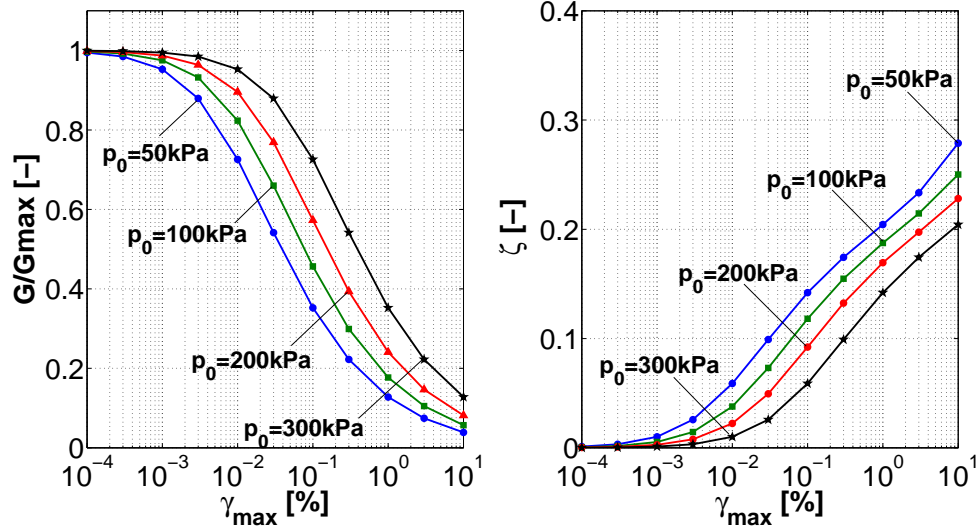
Figure 8: Simulated G/G_{max} and damping curves at varying confining pressure (T=2π s, $G_{max} = 4$ MPa, ν=0.25, M=1.2, k_d=ξ=0, h=$G/(15p_0)$, m=1)

Although the present version of the model is apparently pressure-dependent, it cannot quantitatively reproduce the pressure-sensitiveness of G/G_{max} and ξ curves arising from real experiments and incorporated into some analytical formulas (Ishibashi and Zhang, 1993; Darendeli, 2001). This stems from the fact that the influence of the mean pressure only concerns the plastic component of the model, while constant elastic (and viscous) moduli have been adopted for the initial simulation of only PS loading tests. From this point of view, two easy improvements are possible and mutually compatible:

1. use of hyper- or hypo-elastic laws with variable moduli (Papadimitriou and Bouckovalas, 2002; Andrianopoulos et al., 2010);

2. adoption of p-dependent hardening parameters (i.e. h and m).

In particular, the latter point does not introduce any further difficulty in terms of analytical/numerical treatment, since it only affects the interpolation rule (19). Appropriate $h(p)$

and $m(p)$ relationships could be easily obtained by first calibrating h and m on experimental or analytical cyclic curves for different p values, and then analytically interpolating the parameters values over a meaningful pressure range.

4.2   Influence of the hardening parameters

Figures 9 and 10 show the influence of the hardening parameters h and m on the predicted cyclic curves. In particular, a decrease in either h or m implies a faster development of plastic strains, so that the closely-elastic range tends to disappear and $G/G_{max} < 1$ and $\zeta > 0$ at even $\gamma_{max} = 10^{-4}\%$; conversely, an extended pseudo-elastic behavior can be obtained over a large strain range by increasing the hardening parameters. Apparently, the model ensures high flexibility in terms of cyclic curve shapes, so that the response of standard elastic-plastic models (i.e. with non-vanishing elastic region) can be smoothly approximated (compare for instance the $m = 3$ curves in Figure 10 and the analytical elastic-perfectly plastic frictional curves in Figure 2).
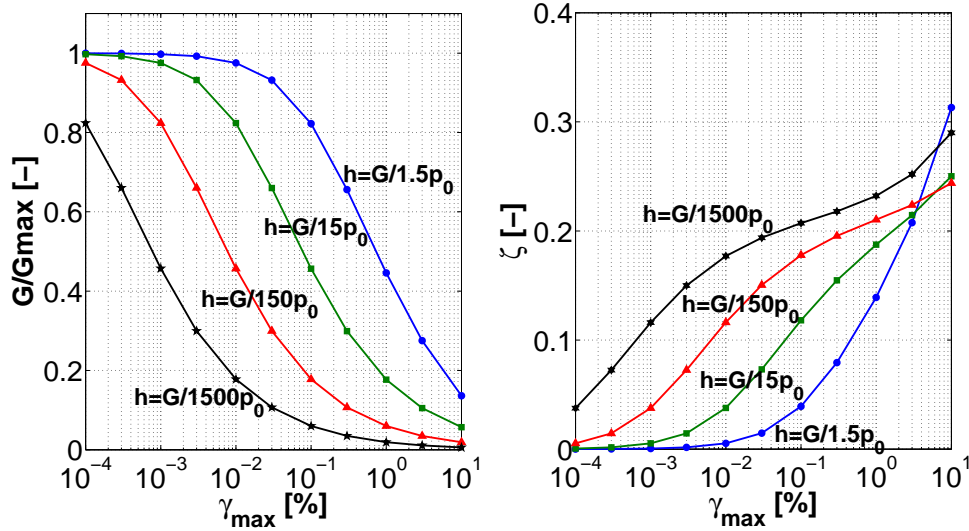
Figure 9: Simulated G/G_{max} and damping curves at varying h (p_0=100 kPa, T=2π s, G_{max} = 4 MPa, ν=0.25, M=1.2, k_d=ξ=0, m=1)

4.3   Influence of the viscous mechanism

The influence of the viscous parameter ζ_0 on the resulting frictional/viscous damping curve is illustrated in Figure 11 (the G/G_{max} is not affected by the parallel viscous mechanism). As was expected, an increase in ζ_0 induce larger values of ζ ($\gamma_{max} \to 0$), as well as a faster increase of the ζ curve at medium/high cyclic strains. Figure 11 confirms the usefulness

21
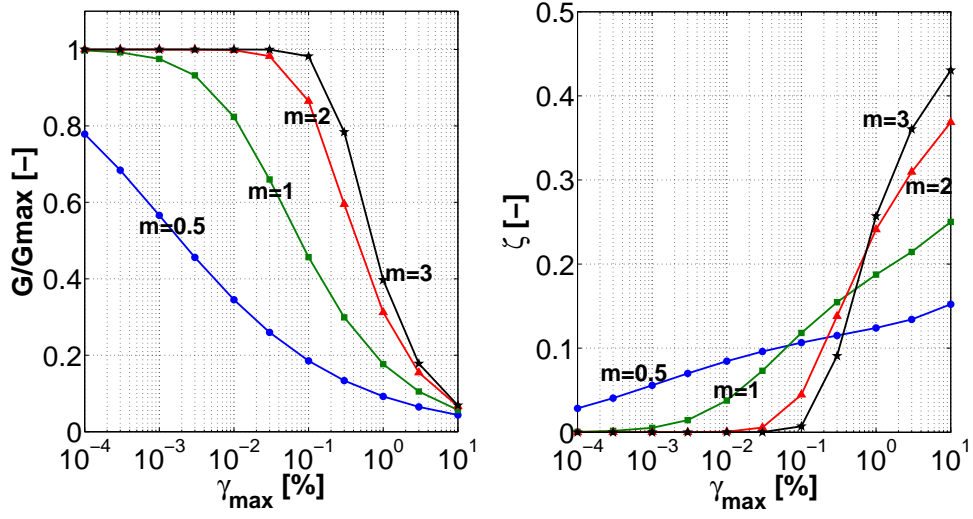
Figure 10: Simulated G/G_{max} and damping curves at varying m (p_0=100 kPa, T=2π s, G_{max} = 4 MPa, ν=0.25, M=1.2, k_d=ξ=0, h=$G_{max}/(15p_0)$)

of the viscous mechanism, which can be exploited as an additional degree of freedom for reproducing the cyclic dissipative soil behavior.
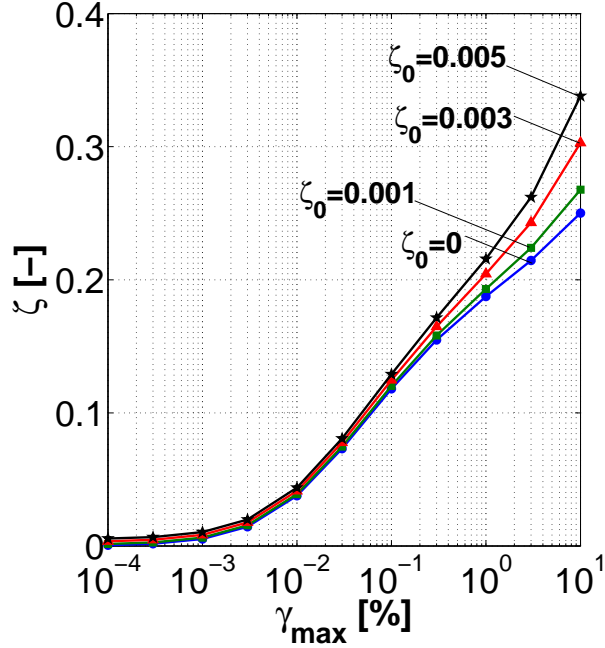
Figure 11: Damping curves simulated at varying ζ_0 (p_0=100 kPa, T=2π s, G_{max} = 4 MPa, ν=0.25, M=1.2, k_d=ξ=0, h=$G_{max}/(15p_0)$, m=1)

4.4 Interaction between volumetric behavior and kinematic constraints

All the above simulations have been performed by inhibiting the elastic-plastic soil dilatancy ($\xi = 0$), which in most cases cannot be done to represent real soil behavior. As previously shown for triaxial loading conditions (Figure 3), in the absence of kinematic boundary constraints, a variation in the volumetric behavior slightly affects only the hardening evolution of the stress-strain response toward the limit shear strength; a similar consideration applies to PS loading conditions, since even in this case the normal confinement is statically determined.

However, computational (FE) models often contain kinematic constraints arising from certain symmetries (consider e.g. plane strain or one-dimensional schemes) (Prevost, 1989; Borja et al., 1999; di Prisco et al., 2012). In addition, for SSI problems, where soil interacts with a (stiff) structural foundations and wall, the soil volume change plays an important role. The presence of kinematic constraints implies that the value of some stress components directly derives from compatibility requirements (e.g. prevented lateral expansion). That means that the local mean confinement is affected by the tendency of the material to dilate or contract. In particular, dilative frictional materials will increase the limit shear stress (with respect to unconfined conditions), while compactive frictional materials will decrease the limit shear stress. Further, not only the limit shear stress, but also the whole pre-failure response depends on the plastic flow rule whenever kinematic constraints are imposed (di Prisco and Pisanò, 2011; di Prisco et al., 2012).

The above considerations suggest that both experimental and numerical results are certainly affected by the kinematics of the system, even though this effect is not easy to be *a priori* quantified in terms of G/G_{max} and ζ curves. The kinematic conditions of an infinite soil layer during 1D shear wave propagation are experimentally approximated through the well known "simple shear (SS) apparatus" (Wood, 2004), in which the soil specimen is cyclically sheared with no lateral expansion allowed. In order to assess how the kinematic confinement influences the cyclic response, stiffness degradation and damping curves are hereafter simulated under SS conditions by varying the volumetric response of the soil; in particular, three different calibrations of the plastic flow rule (6) are considered, namely (i) isochoric ($k_d = \xi = 0$), (ii) compactive ($k_d = M$, $\xi = 1$) and (iii) dilative ($k_d = 0.4$, $\xi = 1$)

The results reported in Figure 12 provide an insight into the possible effect of the volumetric response in combination with constrained loading conditions. In the isochoric case, the PS and the SS curves perfectly match (compare e.g. with the $p_0 = 100$ kPa curves in Figure 8), as, with no plastic expansion (or contraction), the lateral constraints do not affect the mean pressure during the shear loading; conversely, non-negligible SS-PS differences

arise when dilative or contractive materials are considered. As is evident in Figure 12, the discrepancy between isochoric and non-isochoric curves becomes evident at medium/high cyclic strains, i.e. when significant plastifications take place. Indeed, while the mechanical response is barely inelastic, the deviatoric and the volumetric responses are practically decoupled, so that no variation of the normal confinement takes place.

Apparently, the quantitative relevance of this effect strictly relates to the actual dilational properties of the material: soils undergoing significant volume changes under unconfined shear will exhibit a high sensitiveness to boundary constraints. The cyclic interaction between volumetric behavior and kinematic constraints seems to be poorly investigated in literature and is worth remarking for both theoretical and practical motivations. Indeed, the cyclic behavior measured through certain experimental devices (triaxial, biaxial, simple shear, torsional shear, etc) can differ from the mechanical response characterizing other kinematic conditions in boundary value problems, so that the employment of volume-insensitive models (such as the linear equivalent) may lead to inaccurate predictions. In particular, Equation (19) clearly shows that if any relevant p variation arises from the interaction between dilatancy and boundary constraints, a variation in the hardening modulus H and, therefore, the resulting stiffness will also take place. As a consequence, an influence on the global (non-linear) dynamic response is expected in terms of both amplitude amplification and frequency content (Roten et al., 2013). While this aspect is totally disregarded by most modeling approaches in GEE, further work is currently ongoing to quantitatively investigate the role of soil dilatancy in affecting the outcomes of seismic site response (elastic-plastic) analyses.

5   Concluding remarks

An incremental 3D visco-elastic-plastic constitutive model was developed to simulate stiffness degradation and damping in soils under cyclic/dynamic loading. The model is based on an effective-stress formulation with two parallel dissipative mechanisms, purely frictional (elastic-plastic) and viscous.

As far as the frictional mechanism is concerned, a bounding surface formulation with vanishing elastic region was adopted, extending to pressure-sensitive non-associative soils the previous cohesive model by Borja and Amies (1994) for total-stress analyses, but maintaining higher simplicity than later works, such as that e.g. by Andrianopoulos et al. (2010). The main features of the frictional model are: (i) the vanishing yield locus implies an elastic-plastic response at any load levels, as is observed in real experiments; (ii) a minimum number of physically meaningful parameters, which can be easily calibrated on few experimental data; (iii) excellent performance and flexibility in reproducing in the elastic-
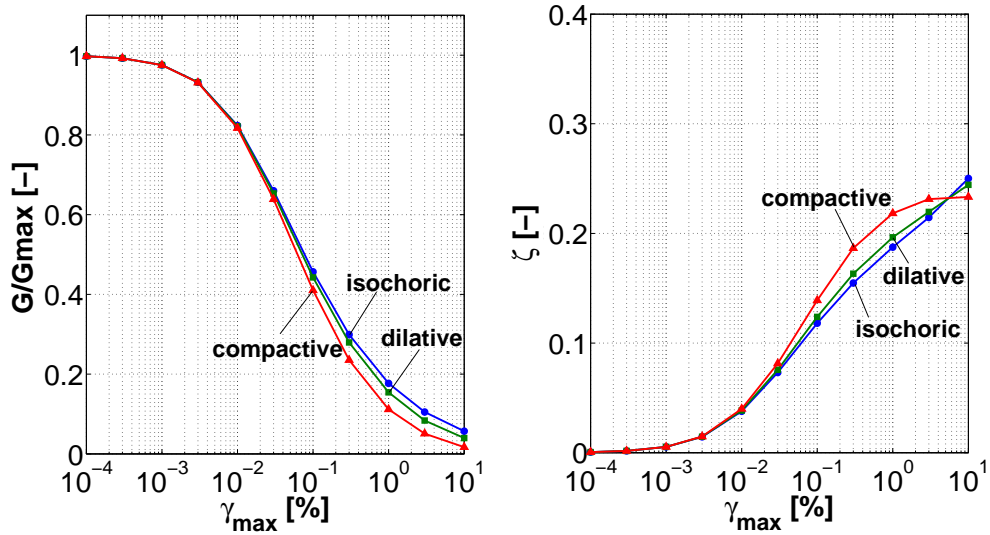
Figure 12: G/G_{max} and damping curves simulated under SS conditions and different volumetric responses (p_0=100 kPa, T=2π s, G_{max} = 4 MPa, ν=0.25, M=1.2, k_d=[1.2, 0.4], ξ=[0,1], h=$G_{max}/(15p_0)$, m=1)

plastic framework the standard stiffness degradation and damping curves. With reference to these latter, the parallel viscous mechanism – easy to be introduced in FE computations – was shown to provide an additional degree of freedom to improve the simulation of the cyclic energy dissipation, as long as the viscous parameter is properly calibrated. As a matter of fact, the viscous mechanism, used here, does physically exist in the form of viscous interaction between the soil solid skeleton and the pore fluid(s), and needs to be taken into account (as for example done here).

Future work will concern the investigation of the model performance under undrained conditions and/or in the presence of non-symmetric loading. Further improvements will be possibly introduced, still with purpose of keeping the model simple and with few material parameters – to be all calibrated on standard experimental data.

Acknowledgment

References

Andrianopoulos, K., A. Papadimitriou, and G. Bouckovalas (2005). Bounding surface models of sands: Pitfalls of mapping rules for cyclic loading. In *Proceedings, 11 th International Conference on Computer Methods and Advances in Geomechanics*, pp. 241–248.

Andrianopoulos, K. I., A. G. Papadimitriou, and G. D. Bouckovalas (2010). Bounding surface plasticity model for the seismic liquefaction analysis of geostructures. *Soil Dynamics and Earthquake Engineering 30*(10), 895–911.

Argyris, J. and H.-P. Mlejnek (1991). *Dynamics of Structures.* North Holland in USA Elsevier.

Bardet, J. P., K. Ichii, and C. H. Lin (2000). EERA, a computer program for equivalent-linear earthquake site response analyses of layered soil deposits. Technical report, University of Southern California.

Bathe, K.-J. (1982). *Finite Element Procedures in Engineering Analysis.* Prentice Hall Inc.

Been, K. and M. Jefferies (1985). A state parameter for sands. *Geotechnique 35*(2), 99–112.

Borja, R. and A. Amies (1994). Multiaxial cyclic plasticity model for clays. *Journal of Geotechnical Engineering 120*(6), 1051–1070.

Borja, R., C. Lin, K. Sama, and G. Masada (2000). Modelling non–linear ground response of non–liquefiable soils. *Earthquake Engineering and Structural Dynamics 29*, 63–83.

Borja, R. I., H. Yih Chao, F. J. Montáns, and C. Hua Lin (1999, March). Nonlinear ground response at Lotung LSST site. *ASCE Journal of Geotechnical and Geoenvironmental Engineering 125*(3), 187–197.

Chopra, A. K. (2000). *Dynamics of Structures, Theory and Application to Earhquake Engineering* (Second ed.). Prentice Hall. ISBN 0-13-086973-2.

Dafalias, Y. (1979). A model for soil behavior under monotonic and cyclic loading conditions. In *Proceedings of the 5th international conference on SMiRT*, Volume K 1/8.

Dafalias, Y. and E. Popov (1977). Cyclic loading for materials with a vanishing elastic region. *Nuclear Engineering and Design 41*(2), 293–302.

Dafalias, Y. F. (1986, September). Bounding surface plasticity. I: Mathematical foundations and hypoplasticity. *ASCE Journal of Engineering Mechanics 112*(9), 966–987.

Dafalias, Y. F. and M. T. Manzari (2004, June). Simple plasticity sand model accounting for fabric change effects. *ASCE Journal of Engineering Mechanics 130*(6), 622–634.

Darendeli, M. (2001). *Development of a new family of normalized modulus reduction and material damping curves.* Ph. D. thesis, University of Texas at Austin.

di Prisco, C., M. Pastor, and F. Pisanò (2012). Shear wave propagation along infinite slopes: A theoretically based numerical study. *International Journal for Numerical and Analytical Methods in Geomechanics 36*(5), 619–642.

di Prisco, C. and F. Pisanò (2011). An exercise on slope stability and perfect elasto-plasticity. *Géotechnique 61*(11), 923–934.

di Prisco, C. and D. Wood (2012). *Mechanical Behaviour of Soils Under Environmentally-Induced Cyclic Loads.* Springer.

E-Kan, M. and H. A. Taiebat (2014). On implementation of bounding surface plasticity models with no overshooting effect in solving boundary value problems. *Computers and Geotechnics 55*, 103–116.

Elgamal, A., Z. Yang, E. Parra, and A. Ragheb (2003). Modeling the cyclic mobility in saturated cohesionless soils. *International Journal of Plasticity 19*(6), 883–905.

Gajo, A. and D. Wood (1999). A kinematic hardening consitutive model for sands: the multiaxial formulation. *International Journal for Numerical and Analytical methods in Geomechanics 23*, 925 – 965.

Hashash, Y. and D. Park (2001). Non-linear one-dimensional wave propagation in the Mississipi embayment. *Engineering Geology 62*(1–3), 185–206.

Hashash, Y. and D. Park (2002). Viscous damping formulation and high frequency motion in non–linear site response analysis. *Soil Dynamics and Earthquake Engineering 22*, 611–624.

Ishibashi, I. and X. Zhang (1993). Unified dynamic shear moduli and damping ratios of sand and clay. *Soils and FOundations 33*(1), 182–191.

Ishihara, K. (1996). *Soil behaviour in earthquake geotechnics.* Clarendon Press, Oxford University Press.

Ishihara, K., F. Tatsuoka, and S. Yasuda (1975). Undrained deformation and liquefaction of sand under cyclic stresses. *Soils and Foundations 15*(1), 29–44.

Kramer, S. L. (1996). *Geotechnical Earthquake Engineering.* Upper Saddle River, New Jersey: Prentice Hall, Inc.

Lade, P. V. (1977). Elastoplastic stress strain theory for cohesionless soil with curved yield surfaces. *International Journal of Solids and Structures 13*, 1019–1035.

Lysmer, J. (1988). SASSI: A computer program for dynamic soil structure interaction analysis. *Report UBC/GT81-02. University of California, Berkeley, CA, USA.*.

Manzari, M. T. and Y. F. Dafalias (1997). A critical state two–surface plasticity model for sands. *Géotechnique 47*(2), 255–272.

Matsuoka, H. and T. Nakai (1974). Stress, deformation and strength characteristics under three different principal stresses. *Proceedings of Japanese Society of Civil Engineers 232*, 59–70.

Mróz, Z., V. A. Norris, and O. C. Zienkiewicz (1978). An anisotropic hardening model for soils and its application to cyclic loading. *International Journal for Numerical and Analytical Methods in Geomechanics 2*, 203–221.

Nova, R. and D. M. Wood (1979). A constitutive model for sand in triaxial compression. *International Journal for Numerical and Analytical Methods in Geomechanics 3*, 255–278.

Papadimitriou, A. G. and G. D. Bouckovalas (2002). Plasticity model for sand under small and large cyclic strains: A multiaxial formulation. *Soil Dynamics and Earthquake Engineering 22*(3), 191–204.

Prevost, J. (1985). A simple plasticity theory for frictional cohesionless soils. *International Journal of Soil Dynamics and Earthquake Engineering 4*(1), 9–17.

Prevost, J. H. (1989). DYNA1D: A computer program for nonlinear site response analysis, technical documentation. technical report no. nceer-89-0025. Technical report, National Center for Earthquake Engineering Research, State University of New York at Buffalo.

Prevost, J. H. and R. Popescu (1996, October). Constitutive relations for soil materials. *Electronic Journal of Geotechnical Engineering*. available at http://139.78.66.61/ejge/.

Roten, D., D. Fäh, and L. Bonilla (2013). High-frequency ground motion amplification during the 2011 tohoku earthquake explained by soil dilatancy. *Geophysical Journal International 193*(2), 898–904.

Schnabel, P., J. Lysmer, and H. B. Seed (1972). Shake – a computer program for equation response analysis of horizontally layered sites. report eerc 72-12. Technical report, University of California Berkeley.

Seed, H. B. and I. M. Idriss (1970). Soil moduli and damping factors for dynamic response analyses. report eerc 70-10. Technical report, University of California Berkeley.

Sett, K., B. Unutmaz, K. Önder Çetin, S. Koprivica, and B. Jeremić (2011). Soil uncertainty and its influence on simulated G/G_{max} and damping behavior. *ASCE Journal of Geotechnical and Geoenvironmental Engineering 137*(3), 218–226. 10.1061/(ASCE)GT.1943-5606.0000420 (July 29, 2010).

Taiebat, M. and Y. F. Dafalias (2008). SANISAND: Simple anisotropic sand plasticity model. *International Journal for Numerical and Analytical Methods in Geomechanics 32*(8), 915–948.

Wang, Z.-L., Y. F. Dafalias, and C.-K. Shen (1990). Bounding surface hypoplasticity model for sand. *Journal of engineering mechanics 116*(5), 983–1001.

Willam, K. J. and E. P. Warnke (1974). Constitutive model for the triaxial behaviour of concrete. In *Proceedings IABSE Seminar on Concrete Bergamo*. ISMES.

Wood, D., K. Belkheir, and D. Liu (1994). Strain softening and state parameter for sand modelling. *Geotechnique 44*(3), 335–339.

Wood, D. M. (2004). *Geotechnical Modelling*. Spoon Press. ISBN 0-415–34304.

Zienkiewicz, O. C., A. H. C. Chan, M. Pastor, B. A. Schrefler, and T. Shiomi (1999). *Computational Geomechanics with Special Reference to Earthquake Engineering*. John Wiley and Sons. ISBN 0-471-98285-7.

Zienkiewicz, O. C. and R. L. Taylor (1991). *The Finite Element Method* (fourth ed.), Volume 1. McGraw - Hill Book Company.

A   Derivation of Equation (28)

Under PS loading conditions (pure shear at constant mean pressure), Equation (16) produces the following simple expression for β:

$$\beta = \frac{\tau_{lim} - \tau}{\tau - \tau_0} \tag{29}$$

where $\tau_{lim} = Mp_0/\sqrt{3}$ and p_0 is the initial (and constant) mean pressure. Equation (12) can be easily specified for PS loading:

$$dq = \sqrt{3}d\tau = \sqrt{\frac{2}{3}}H\|de_{ij}^p\| = \sqrt{\frac{2}{3}}H\frac{d\gamma^p}{\sqrt{2}} \implies d\tau = \frac{H}{3}d\gamma^p \tag{30}$$

so that the following form of the PS elastic-plastic response results:

$$d\gamma = d\gamma^e + d\gamma^p = \frac{d\tau}{G_{max}} + \frac{3d\tau}{H} \tag{31}$$

and, after substituting (29) into (19):

$$d\gamma = \frac{d\tau}{G_{max}} + \frac{3d\tau}{p_0 h\beta^m} = \frac{d\tau}{G_{max}} + \left(\frac{\tau - \tau_0}{\tau_{lim} - \tau}\right)^m \frac{3d\tau}{p_0 h} \tag{32}$$

Integration over a strain interval between two stress reversals ($\gamma \in [-\gamma_{max}; \gamma_{max}]$) yields:

$$2\gamma_{max} = \frac{2\tau}{G_{max}} + \frac{3}{hp_0}\int_{-\tau}^{\tau}\left(\frac{\tau' + \tau}{\tau_{lim} - \tau'}\right)^m d\tau' \tag{33}$$

where $\tau_0 = -\tau$ has been set. Straightforward variable changes lead to:

$$1 = \frac{G}{G_{max}} + \frac{3}{2hp_0\gamma_{max}}\int_0^{2G\gamma_{max}}\left(\frac{\tau''}{\tau_{lim} - \tau'' + G\gamma_{max}}\right)^m d\tau'' \tag{34}$$

$$1 = \frac{G}{G_{max}}\left[1 + \frac{6G_{max}}{hp_0\gamma_{max}}\int_0^{\gamma_{max}}\left(\frac{\gamma}{\tau_{lim}/G - 2\gamma + \gamma_{max}}\right)^m d\gamma\right] \tag{35}$$

It is worth highlighting that two approximations are implicitly contained in Equation (35): (i) the integration over the first loading cycle does not exactly reproduce the stabilized cyclic response (because of the aforementioned Masing effect); (ii) a symmetric loading cycle in terms of shear strain does not in general ensure the symmetry of the corresponding shear stress range (as it is assumed in Equation (33)). However, such approximations do not prevent reasonable values for the hardening parameters h and m to be obtained.